Dynamical coupling of neutrals and ions in the high-latitude *F* region: Simultaneous FPI and HF radar observations at Syowa Station, Antarctica

Takeshi Sakanoi,[1] Hiroshi Fukunishi,[1] Shoichi Okano,[1] Natsuo Sato,[2] Hisao Yamagishi,[2] and Akira S. Yukimatu[2]

Received 2 May 2001; revised 21 November 2001; accepted 29 April 2002; published 21 November 2002.

[1] Simultaneous measurements of neutral winds and plasma drifts have been carried out to clarify the local neutral-ion coupling processes in the auroral *F* region. High-resolution maps of thermospheric winds and plasma drifts were made using data obtained by the Fabry-Perot Doppler Imaging System (FPDIS) and by the Syowa-South HF radar, respectively, both installed at Syowa Station (66.4° in magnetic latitude), Antarctica during the solar minimum period in 1996. We made case studies for two nights: one on 13 May 1996 during a rather quiet period including the growth phase of a substorm, and the other on 24–25 April 1996 during a moderately active period. From 2000 to 2200 UT on 13 May, the velocities of neutral winds and plasma drifts showed similar time variations: a negative excursion followed by a positive excursion. However, the variations of plasma drifts preceded those of neutral winds with a time lag of ~30 min, and plasma drift velocities were about 7–10 times greater than neutral wind velocities. Therefore, it is suggested that the variations of neutral winds were driven by the ion drag force. To interpret results of the 13 May case, we simulated the relationship between neutral winds and ion drifts by including the effect of auroral heating, such as Joule and particle heating. The results suggest that strong neutral winds were driven by the ion drag and the pressure gradient force induced by auroral heating. In contrast, in the case of 24–25 April, no similarity was found between neutral winds and plasma drifts. Although it is difficult to specify sources for the discrepancy, some possible origins are proposed. For example, if the pressure gradient force is much greater than the ion drag force as in the case of disturbed period, neutral wind variations become independent of plasma drift variations. The discrepancy is also caused by the existence of vertical winds associated with active aurora. *INDEX TERMS:* 0335 Atmospheric Composition and Structure: Ion chemistry of the atmosphere (2419, 2427); 0358 Atmospheric Composition and Structure: Thermosphere—energy deposition; 2704 Magnetospheric Physics: Auroral phenomena (2407); *KEYWORDS:* ionosphere, thermosphere, *F* region, neutral wind, plasma drift, aurora

Citation: Sakanoi, T., H. Fukunishi, S. Okano, N. Sato, H. Yamagishi, and A. S. Yukimatu, Dynamical coupling of neutrals and ions in the high-latitude *F* region: Simultaneous FPI and HF radar observations at Syowa station, Antarctica, *J. Geophys. Res.*, *107*(A11), 1388, doi:10.1029/2001JA007530, 2002.

1. Introduction

[2] Ionosphere-thermosphere (IT) interaction processes at high latitudes have been investigated theoretically and experimentally with immense interest. These interaction processes show complicated behaviors due to the presence of different external energy sources driving the motions of neutrals and plasmas. Thermospheric neutrals are dynamically coupled with ions through collisions, called ion drag. In addition, the motions of neutrals are also driven by nonelectromagnetic forces, such as pressure gradient force, Coriolis force, momentum advection, and viscosity. These driving forces on neutrals show significant temporal and spatial variations; small-scale pressure gradient force can be produced by local Joule heating, while day-to-night pressure gradient force produces the global-scale circulation of neutrals. On the other hand, ionospheric plasma motions are mostly controlled by the electromagnetic force of electric field transferred from the magnetosphere, and the global convection shows a two-cell pattern. Thus, these plasma motions are strongly affected by magnetic activities associated with magnetospheric substorms. In addition, ionospheric plasmas can also be driven by the neutral drag force due to collisions between neutrals and ions.

[3] In order to understand the IT coupling processes, various studies have been made so far both in global and

[1]Department of Geophysics, Graduate School of Science, Tohoku University, Sendai, Japan.
[2]National Institute of Polar Research, Kaga, Itabashi, Tokyo, Japan.

0148-0227/02/2001JA007530$09.00

local scales. Concerning the global-scale neutral wind system, experimental studies using DE-2 satellite data have shown a two-cell flow pattern of horizontal winds in high latitude that is similar to the ion convection pattern [e.g., *Hays et al.*, 1984; *Killeen and Roble*, 1988]. *Killeen et al.* [1985] examined the large-scale relationship between neutral winds and ion drifts during a solar maximum period, and showed that variations of neutral winds are similar to those of ion drifts with, however, a reduction in magnitude and with much less evident spatial structure. *Killeen et al.* [1984] also suggested that Joule heating plays an important role in the IT coupling by increasing the temperatures of neutrals and ions. However, note that these data describe a snap shot of wind variations along a satellite track.

[4] The global IT coupling was also investigated theoretically by thermospheric general circulation models [e.g., *Fuller-Rowell et al.*, 1994; *Killeen and Roble*, 1984; *Deng et al.*, 1993; *Lu et al.*, 1995; *Thayer et al.*, 1995b; *Peymirat et al.*, 1998]. These studies demonstrated that the thermospheric winds produce a dynamo effect through neutral-ion collisions and contribute to the overall electrodynamics of the coupled magnetosphere-ionosphere-thermosphere system. However, the spatial resolution of such global models is typically 300–500 km, which is much larger than the scale of local auroral structures and electrojets.

[5] On the other hand, the local IT coupling at high latitudes has been examined using experimental data from sounding rockets [e.g., *Brinkman et al.*, 1995; *Odom et al.*, 1997], and from ground-based radars [e.g., *Fujii et al.*, 1998a, 1998b, 1999], and from optical Fabry-Perot spectrometers (FPS) [e.g., *Rees et al.*, 1984, *Batten and Rees*, 1990; *Hernandez et al.*, 1990; *Conde and Smith*, 1995, 1998; *Conde et al.*, 2001; *Steen et al.*, 1988; *Smith et al.*, 1994; *Ishii et al.*, 1999, 2001; *Dyson et al.*, 1997; *Sakanoi and Fukunishi*, 1999]. Using an imaging type FPS, *Conde and Smith* [1998] reported small-scale variations of neutral winds in the auroral region. Although *Conde and Smith* [1998] confirmed that average horizontal wind patterns are consistent with the results obtained from the global thermospheric model, considerable differences are found in the late evening and midnight sectors, depending on auroral activities, suggesting the existence of vertical winds. The statistical study on the relationship between vertical winds and optical aurora was also reported by *Ishii et al.* [2001]. *Thayer et al.* [1995a] reported a relationship between neutral and ion motions and its dependence on IMF conditions using FPS and digital ionosonde data obtained in the polar cap *F* region, and showed that neutral winds in the polar cap are driven not only by the ion drag force but also by the day-to-night pressure gradient force. The local IT coupling was also studied by using 2- or 3-dimensional regional models [*Lyons and Walterscheid*, 1985; *Walterscheid and Lyons*, 1992; *Sun et al.*, 1995]. However, local dynamics of neutrals and ions is not well understood compared with the global dynamics, since simultaneous measurements of neutrals and ions have been scarcely carried out in the auroral region.

[6] In the present study, we focus on the local relationship between the motions of neutrals and ions. The observations reported here were carried out at Syowa Station, Antarctica (69.00°S and 39.58°E in geographic coordinates and 66.4° in magnetic latitude) under solar minimum conditions in 1996. Spatially-resolved neutral winds were obtained by a Fabry-Perot Doppler imaging system (here, referred to as FPDIS) from Doppler shift of auroral OI 630 nm emission with a peak intensity at ~250 km altitude. Plasma drift motions were obtained by the HF radar (here, referred to as the Syowa-South HF radar) ranging over 3000 km poleward of Syowa Station. These imaging measurements of neutral winds and ion drifts provide us with a unique opportunity to examine the local IT coupling processes in detail. Since the typical spatial resolutions of neutral wind and ion drift measurements were several tens of km, these data can contribute to evaluating the effects of small-scale variations on the parameters of the global thermosphere ionosphere general circulation models.

2. Instrumentation and Data Analysis

2.1. Fabry-Perot Doppler Imaging System

[7] FPDIS is an imaging Fabry-Perot spectrometer developed originally in 1989 and improved in 1993 and 1995. Its Fabry-Perot etalon is a 116-mm-aperture capacitance-stabilized type with a spacing of 12 mm. Over two orders of interference fringes are focused on at the photocathode of a proximity focused photon counting imager (PFPCI) with three-stage multichannel plates. The fringe image is conjugate with a field-of-view (FOV) on the sky. The center wavelength and the full-width at half maximum of the interference filter used to isolate the auroral OI 630 nm line are 630.1 nm and 1.0 nm, respectively. An image on the fluorescent screen of PFPCI is optically coupled to a CCD camera with a video frame rate. Then the video signals from the CCD camera are digitized to 512 × 480 pixel data, discriminating dark noise with an appropriate threshold level, and obtained digital data are integrated by an image data processor in real time.

[8] Observations of neutral winds and temperatures using this FPDIS have been carried out at Syowa Station, Antarctica during winter periods in 1990, 1994, and 1996. In 1990 the measurements were made with a prototype FPDIS with a FOV of 165°, which employed a photon imaging head (PIH) instead of PFPCI [*Nakajima et al.*, 1995]. After that, PIH was replaced by the PFPCI for reducing image distortion. Observations were made with an improved FPDIS with the same FOV of 165° in 1994 [*Kubota*, 1996]. On the other hand, observations in 1996 presented here were carried out by using a combination of a wide-angle objective lens (FOV = 42°) and a slant mirror in the front of objective lens in order to observe high-spatial resolved neutral winds and temperatures in the *F* region covered by the HF radar. The center of the FOV of FPDIS is approximately directed toward the FOV of the Syowa-South HF radar. The schematic geometry of observations is presented in Figure 1. Although the peak of OI 630 nm emission is generally located around 250 km altitude, the thickness of the emission layer varies within 100 km associated with auroral particle precipitation [*Solomon et al.*, 1988]. As shown schematically in Figure 1, observed neutral winds are averaged values along a line-of-sight path in the emission layer.

[9] The calibration of the etalon and the optical system was made using a frequency stabilized He-Ne laser (λ = 632.8 nm). Calibration fringe data were routinely recorded

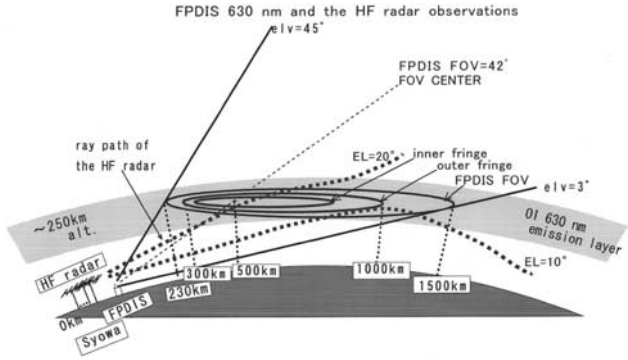

Figure 1. Schematic illustration of observations showing the field-of-view of FPDIS (solid line) and the ray path emitted from the HF radar (dotted line). Simultaneous neutral wind and plasma drift data in the *F* region are obtained in the range between ~400 and 1000 km from Syowa.

every hour during observations for monitoring drift of the etalon.

2.2. Estimations of Neutral Winds and Temperatures

[10] Since the amounts of Doppler shifts and broadening of auroral emission lines due to neutral winds and temperatures are extremely small, we performed a detailed analysis of measured fringe data. Procedures of data analysis given as follows: (1) A fringe center is determined using calibration laser fringes. (2) Using the determined center position, each fringe image is divided into 24 sectors with 15 degrees separations in the azimuthal directions, and then it is converted to 24 sliced profiles. Since two fringes are obtained by FPDIS, the total number of sliced profiles is 48 (24 for each of the inner and outer fringes). These sliced profiles are obtained from each fringe image with a typical exposure time of 10–20 min and this time determines the time resolution of neutral winds and temperature measurements. (3) To estimate the line-of-sight (LOS) component of neutral winds, the peak fringe position is determined by fitting a Gaussian function to each sliced profile using a nonlinear least squares method. LOS wind velocity is estimated by comparing the peak position with that of a reference ''wind-zero'' fringe. The reference wind-zero fringe used here was obtained during a night when the sky was uniformly cloudy and auroral activity was low, assuming that auroral/airglow emission light scattered by clouds has no Doppler shift. In the present study we regard the velocity as the LOS component of horizontal neutral wind velocity assuming that a vertical wind is negligible. (4) To estimate neutral temperatures, we use a numerical technique based on a truncated Fourier series that is originally developed by *Killeen and Hays* [1984], and also used by *Nakajima et al.* [1995]. Fourier coefficients describing the instrument function are obtained using calibration fringes recorded with the He-Ne laser (632.8 nm) as source, and they properly converted to the values at OI 630 nm interpolating both phase and power. The use of a quasi-linear least squares fitting process involving the use of matrices allows an efficient and accurate data reduction [*Killeen and Hays*, 1984]. Temperatures are determined by interpolating Fourier coefficients that produce a best fit curve to observed fringe.

[11] Errors in neutral winds and temperatures are classified into random/variable errors and systematic offsets. According to the detailed analysis by *Nakajima et al.* [1995], random errors are better than 15 m/s for winds, and better than 80 K for temperatures, respectively, considering that photon counts at fringe peaks are generally greater than 800 counts per pixel. In addition, apparent neutral winds can be produced by the shifting of fringe peaks due to large spatial gradients of auroral intensity in the FOV [*Conde and Smith*, 1998]. Its error is negligible when intensity gradient is not steep, such as a case of a diffuse aurora. However, from a numerical simulation by *Kubota* [1996] with 630 nm fringes, error can become as much as 100–200 m/s in a case of active aurora. Further, shifts of fringe peaks due to drift of the etalon spacing may occur, but this amount can be corrected by calibration made routinely every hour. In general, this method corrects the etalon spacing drift exactly except for a period of steep change of room temperature ($\Delta T > 5$ K/hour, empirically). Consequently, we used the data obtained only for periods when the room temperature was kept stable. As for the systematic offsets of neutral winds which depend on accuracy in determination of a wind-zero fringe and its center position are estimated to be better than 100 m/s.

[12] The systematic offsets of derived neutral temperatures exist for the following reason. It is likely that the focus position of calibration fringe was slightly different from that of auroral fringe since calibration laser data were obtained without an interference filter. This effect leads to the error in absolute values of neutral temperatures. Compared with neutral temperatures of the MSISE-90 model, negative offsets (less than ~200 K) seem to be involved in the estimated temperatures. However, we can discuss relative temporal changes of neutral temperatures since the offsets are thought to be almost constant at each position of fringes throughout an observation period.

2.3. Syowa-South HF Radar

[13] The Syowa-South HF radar comprises part of the SuperDARN (Dual Auroral Radar Network) designed to observe ionospheric convection patterns over large spatial extent [e.g., *Greenwald et al.*, 1995]. The SuperDARN radars are operated at frequencies between 8 and 20 MHz and measure coherent backscattered echo power and Doppler spectral characteristics of decameter-range field-aligned irregularities in the *E* and *F* regions. At *F* region level, LOS Doppler velocity of irregularities gives a measure of the E × B plasma drift velocity. On ordinary measurements of the Syowa-South HF radar, a wide FOV of ~52° is divided into 16 azimuthal sectors as scanned by a narrow (~3.25°) beam with a scan period of 2 min, and the backscatter echo signals are range-gated in step of 45 km starting from 180 km range. The center of the FOV is directed ~21° eastward from the geographic south. The ray paths of HF waves emitted from Syowa-South HF radar with elevation angles (EL) of 10 and 20 are shown schematically in Figure 1. Generally, a wave with small EL is refracted a little downward in the bottomside of the *F* region [*Greenwald et al.*, 1995], while a wave with large EL penetrates into the topside ionosphere [*Ogawa et al.*, 1990]. Then, the HF

wave is scattered in the *F* region where the radar wave vector is almost perpendicular to the geomagnetic field. From a ray tracing analysis of a wave emission from the Syowa-HF radar [*Ogawa et al.*, 1990], backscatter echoes from the *F* region are expected in the range greater than ~400–500 km from Syowa. Therefore, simultaneous measurements of neutral winds and plasma drifts in the *F* region are made in the range greater than ~400–500 km from Syowa as illustrated in Figure 1.

3. Observations

3.1. Data Selection

[14] Simultaneous observations of neutral winds, temperatures, and plasma drifts at Syowa were carried out on 38 nights during the period from April through October 1996. Unfortunately, several of 16 HF radar antennas were damaged by gusty blizzards that attacked Syowa in May and June 1996. In addition, auroral activities were extremely low because of solar minimum condition. As a result, backscatter echoes obtained by the Syowa-South HF radar were generally weak in 1996. However, clear backscatter echoes were obtained by the HF radar on two nights of 13 May and 24 April in 1996 when FPDIS was operated simultaneously. Here we will present the results obtained on these two nights: 13 May during a rather quiet period including the growth phase of a substorm and 24 April during a moderately active period. We will also describe IMF conditions on these nights using WIND data in which time is corrected as considering solar wind velocities and the distance between the spacecraft and the Earth.

[15] To recognize the behavior of plasma convection flow, the two-dimensional vector plot of plasma drift is made from a single HF radar data with some assumptions such as the L shell invariance in the velocity field [*Ruohomiemi et al.*, 1989]. Although such method estimating two-dimensional vector is useful, the error in velocity increases with increasing convection flow curvature with respect to the L shell [*Freeman et al.*, 1991]. *Freeman et al.* [1991] also reported that it is impossible to decide accuracy of convection vectors at various locations. In both cases on 13 May and 24 April, we consider that the estimation of convection vector by the method is fraught with difficulties since the radar echoes obtained from the HF radar were seen in rather limited area (less than ~300 × 500 km). Moreover, the mesoscale (less than 500 km) velocity reversal of plasma drifts seemed to occur in the 13 May case. Since the HF radar and the FPDIS observed LOS velocities of plasma drifts and neutral winds, respectively, we can compare neutral winds with plasma drifts without any assumptions. Therefore, the LOS velocity maps of neutral winds and plasma drifts will be shown in the following section. Further, in section 4.2, by using those LOS velocities, the relationship between neutral winds and ion drifts will be solved from the calculation based on the momentum equation of neutrals.

3.2. 13 May 1996 Case

[16] Auroral and geomagnetic conditions on 13–14 May are given in Figure 2. Note that universal time (UT) is almost the same as magnetic local time (MLT) at Syowa Station. The IMF Bz component obtained from WIND data

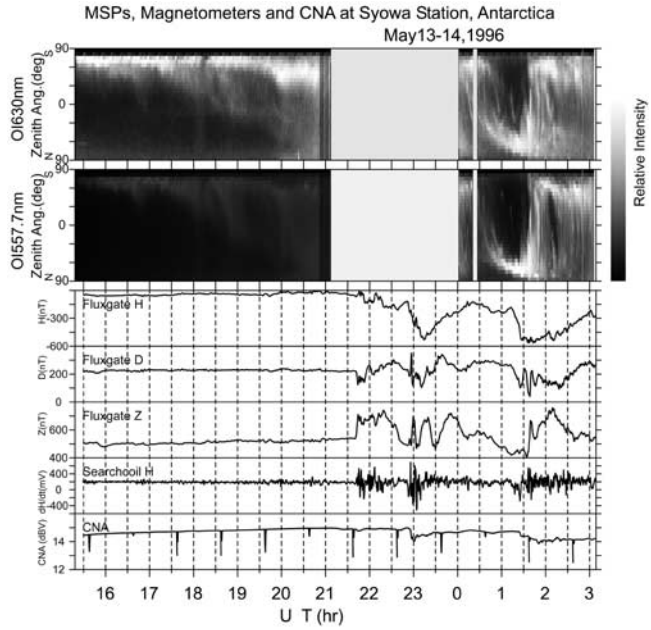

Figure 2. Summary plots of auroral and geomagnetic activities obtained on 13–14 May 1996 at Syowa. Top two panels show auroral keograms at emissions of 630 nm and 557.7 nm, respectively. The ordinate represents viewing angle along the magnetic meridian with S corresponding to the south horizon, namely, the magnetic poleward. From the third to fifth panels, the H, D, and Z components of fluxgate magnetometer data are indicated. The sixth panel shows the H component of searchcoil magnetometer data. The bottom panel indicates the cosmic noise absorption (CNA) data obtained by a riometer.

showed mostly positive (0–7 nT) before 2000 UT, and ~0 nT or slightly negative from 2000 UT on 13 May through 0030 UT on 14 May, and a few nT negative after 0030 UT. Before the first auroral break up at ~2140 UT, geomagnetic activity was quite low. From auroral keograms obtained by meridional scanning photometers (MSP), stable 630 nm auroral emissions existed in the poleward direction, and slightly brightened after 2000 UT. This brightening is likely to be related to an IMF Bz change from positive to zero as described above. Although there was no MSP data from ~2100 to 0000 UT owing to exchange of magnetic recording tape, the first breakup was identified by geomagnetic data at 2140 UT and all-sky camera data which are not displayed in this figure. Following this activity, the second and third breakup occurred at ~2250 UT and ~0130 UT on 14 May, respectively.

[17] Clear backscatter echoes were obtained by the Syowa-South HF radar from ~2000 to 2130 UT during a quiet period including the growth phase of a substorm in the range between ~400 and 1000 km poleward of Syowa. The summary plots of simultaneous neutral wind, plasma drift, and 630 nm auroral image data are shown in Figure 3. Note that all plots are not displayed in Figure 3 due to a limitation of space although neutral wind and plasma drift data were obtained at time intervals of 10–20 min and 2 min, respectively. It is clear at 2015 UT that plasma drifted in the direction mostly away from Syowa with speeds of 400–

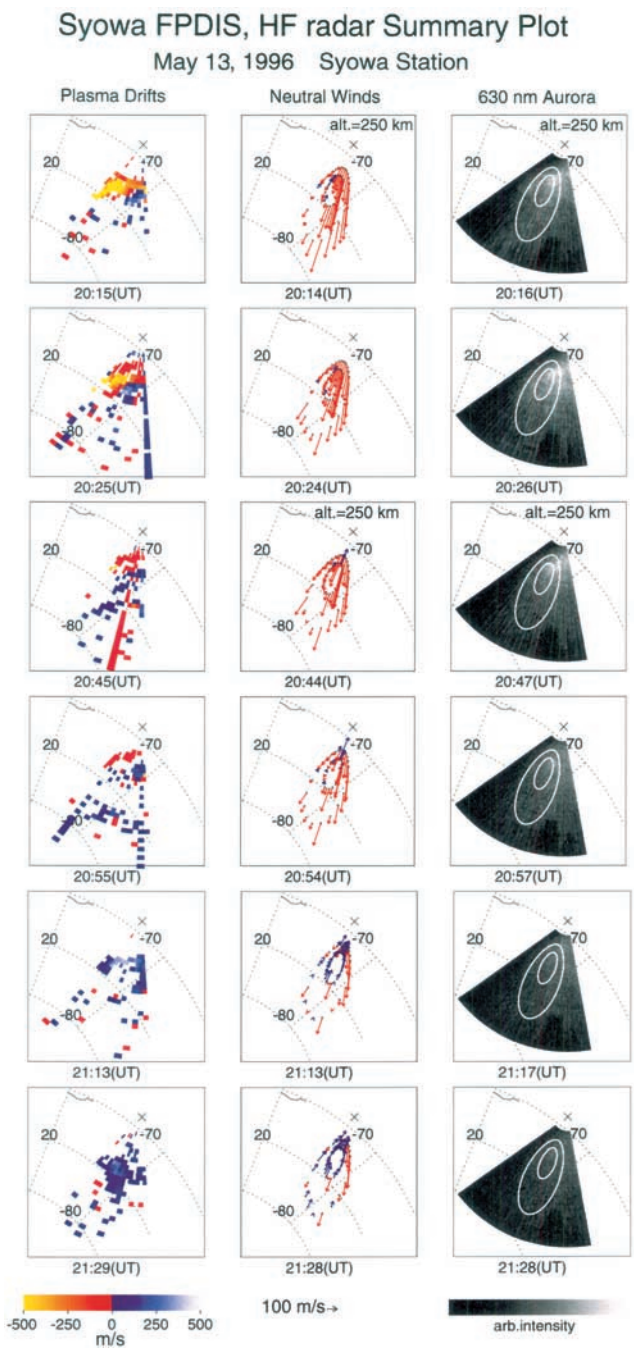

Figure 3. Summary plots of simultaneous measurements between plasma drifts (left-hand line), neutral winds (middle line) and auroral emission distributions at 630 nm (right-hand line) obtained on 13 May 1996 shown in the geographical coordinate system. The location of Syowa is indicated by the cross mark. In the plasma drift data, warm and cold colors represent the drift direction away from Syowa and that toward Syowa, respectively. In neutral wind data, assuming the emission altitude to 250 km, the wind velocities are indicated by the length of arrow, while red and blue colors indicate the wind direction away from Syowa and that toward Syowa, respectively. The 630 nm aurora distributions were obtained by the wide-angle monochromatic imager at Syowa.

600 m/s as indicated by red and yellow colors. At this moment, similar to plasma drifts, neutral wind directions were also away from Syowa indicated by red arrows. However, a small region characterized by equatorward plasma drifts, indicated by blue and white colors, was also identified around 73°S latitude and 44°E longitude at 2015 UT. Auroral image data at this time showed occurrence of a weak diffuse aurora poleward of Syowa.

[18] Ten minutes later, both regions of poleward and equatorward plasma drifts shifted slightly westward with the LOS velocity reversal of plasma drift between those two regions at 2025 UT (see left of the second panels from the top in Figure 3). At the same time, however, neutral wind directions were still poleward in the whole area of FOV at 2024 UT (see the middle of the second panels). After 2024 UT, both regions of poleward and equatorward plasma drifts shifted gradually westward. As a result, plasma drift directions became equatorward in almost the whole region after 2113 UT. On the other hand, the directions of neutral winds were mostly poleward until 2054 UT, then changed to equatorward after ~2113 UT. By comparing those variations between plasma drifts and neutral winds, it is obvious that the variations of neutral winds followed the variations of plasma drifts.

[19] The variations of plasma drifts and neutral winds are interpreted as follows. Considering the fact that at 2015 UT the LOS velocities of plasma drifts were positive/negative on the eastern beams and negative on the western beams, the plasma convection was westward almost along L-shells. Then, the convection changed its direction and strength with time: in particular, the direction rotated clockwise, resulting in that all the LOS velocities on all the beams at 2129 UT were positive. On the other hand, the neutral wind velocity maps at 2014 UT indicate the wind vectors to direct toward SE or ESE since the negative vectors were higher in the eastern half of the FPDIS FOV. In Figure 3, the precise behavior of neutral wind variations is not recognized well although positive vectors of neutral winds were gradually increased in time. Thus, the maps of differential velocities, that is, the accelerations of neutral winds, is shown in Figure 4. It is found that significant acceleration of neutral winds started from the period of 2014–2024 UT: negative acceleration existed in the eastern side of inner fringe (that is, in the near range), while positive acceleration existed in the westward of outer fringe (that is, in the distant range). The acceleration calmed down in the period of 2024–2044 UT. Then strong acceleration occurred in the period of 2044–2054 UT, that is, positive acceleration in the eastern side, and negative/positive acceleration in the western side. In the following periods, positive acceleration existed in all the area of FPDIS FOV with decreasing its magnitude. Since the behavior of neutral wind acceleration map is similar to that of LOS velocity map of plasma drift, it is concluded that the direction of neutral winds also rotated clockwise as well as that of plasma drifts. From the momentum equation of neutrals shown later in section 4, it is reasonable that there is a correlation between the acceleration of neutral winds and the ion drift velocity.

[20] To examine the relationship between plasma drifts and neutral winds in detail, we plotted time series of plasma drift and horizontal neutral wind at locations A–D in Figure 5. A data point at a certain time is an average value

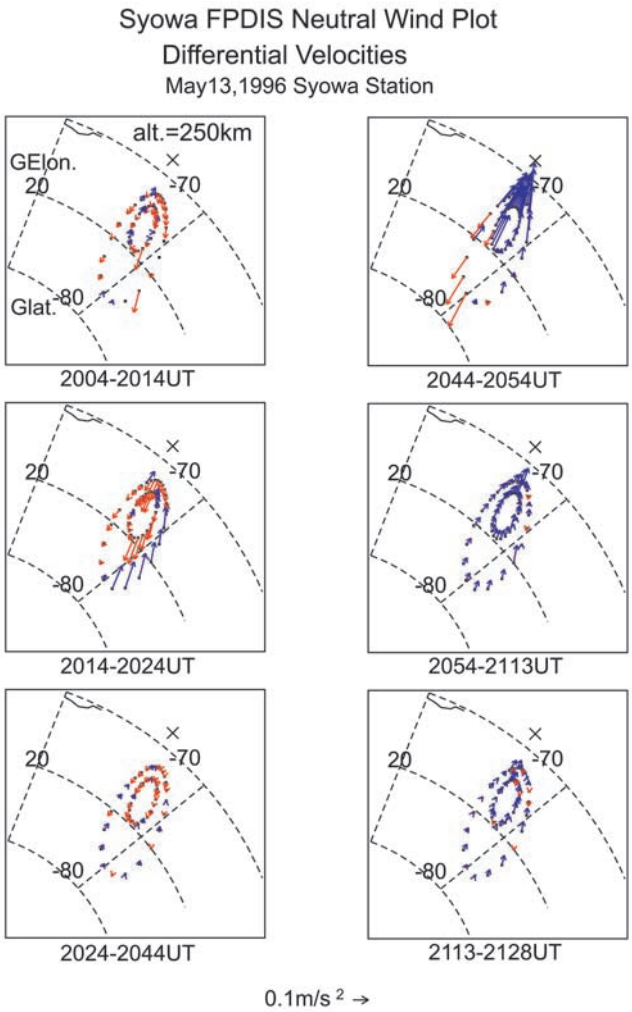

Figure 4. Time variations of differential velocities of neutral winds, that is, the acceleration of neutral winds, obtained from 2004 to 2128 UT on 13 May 1996, corresponding to the period shown in Figure 3. Each map shows the distribution of differential velocities obtained from the variation of LOS velocities at each data point during the period shown in the bottom of each map. Red and blue arrows indicate the negative and positive differential velocities, respectively, where the positive differential velocity shows the neutral wind acceleration in the direction away from Syowa.

on each location. Here, the horizontal neutral wind was obtained by $U_{LOS}/\sin(\theta)$, where U_{LOS} is the line-of-sight component to of neutral winds, and θ is the zenith angle, and also the average value was subtracted for each variation. Neutral temperatures obtained from outer fringe data (namely, locations A and D) are represented in this figure since inner fringe positions were located too close to the center of the fringe pattern and their sliced profiles were overlapped around the center, although the peak positions of inner fringe were clearly determined. Locations A, B, C, D are shown at the bottom in Figure 5. It is evident that neutral winds showed bipolar time variations, namely, a negative excursion (away from Syowa; mostly poleward) followed by a positive excursion (toward Syowa; mostly equator-

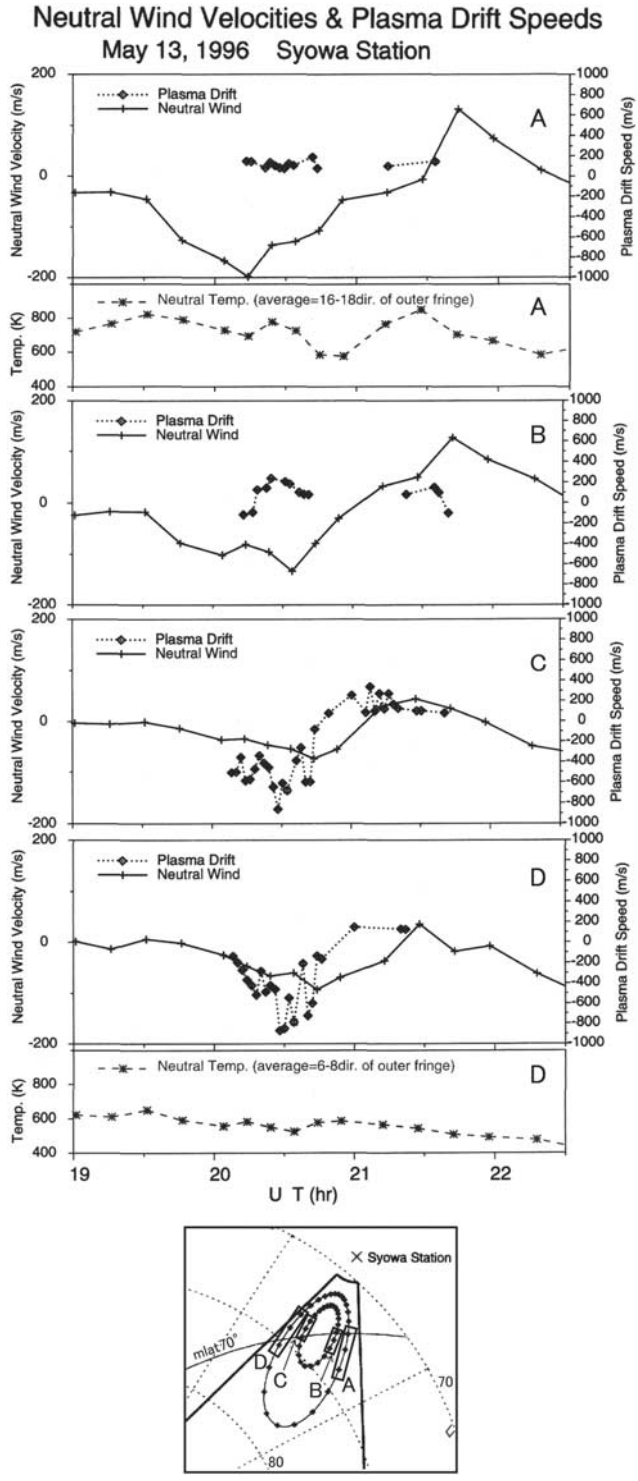

Figure 5. Time variations of simultaneous horizontal neutral wind velocities and plasma drift velocities in the line-of-sight direction at selected 4 locations obtained from 1900 to 2230 UT on 13 May 1996. The selected 4 locations indicated as A, B, C, D are shown in the bottom map. Here, the horizontal neutral wind was obtained by $U_{LOS}/\sin(\theta)$, where U_{LOS} is the line-of-sight component to of neutral winds, and θ is the zenith angle, and also the average value was subtracted for each variation. The second and sixth panels show the variations of neutral temperatures obtained at locations A and D, respectively.

ward), in all locations. The variation of neutral wind speeds was ∼−130 to +120 m/s at B, and ∼−80 to +60 m/s at C. Also bipolar variations of plasma drifts similar to neutral wind variations were seen at C and D although these variations slightly preceded neutral wind variations. The time lag between the variations of neutral winds and plasma drifts was about 30 min which was estimated from the peaks of bipolar variations or the reversal times of neutral wind and plasma drift directions as seen at C. The plasma drift speeds at C were ∼−850 to 400 m/s which were about 7–10 times greater than those of neutral winds. Regarding the plasma drifts at A and B, we see positive drifts after ∼2000 UT. Considering that the westward motion of plasma drift pattern is seen in Figure 3 and also that usual plasma convection in auroral zone around 2000 UT is westward, it is supposed that the plasma drifts were negative before ∼2000 UT although there were no backscatter echoes during this time interval. In that case, the speed of zonal (westward) motion of plasma drift pattern is estimated to be ∼60 m/s from the time delay between the positive peaks at B and C. We also see a gradual decrease in neutral temperatures after ∼2045 UT. This gradual decrease is similar to those in auroral intensities during this period as seen in Figure 3.

3.3. 24 April 1996 Case

[21] In this night auroral and geomagnetic activities were almost comparable to those on 13–14 May. However, backscatter echoes of the HF radar were obtained only during rather disturbed periods. Figure 6 shows auroral and geomagnetic conditions on 24–25 April 1996. The IMF Bz component showed 0–4 nT negative excursion before 2300 UT, and variable from 2300 UT on 24 April to 0200 UT on 25 April except for about 4 nT negative excursion around ∼0030 UT and a few nT negative excursion after 0200 UT. Two enhancements in auroral and geomagnetic activities were identified at ∼1945 UT on 24 April and at ∼0015 UT on 25 April, while 630 nm aurora appeared continuously poleward of Syowa during this night. Backscatter echoes of the HF radar were observed during a period from 2200 UT on 24 April to 0000 UT on 25 April, and during a period from 0100 to 0230 UT on 25 April. The summary plots of simultaneous neutral wind, plasma drift, and 630 nm auroral image data are shown in Figure 7. From 630 nm aurora image data, it is obvious that variations of auroral intensities were more active on this night than the previous case. From HF radar data, it is found that plasma drifted mostly in the direction toward Syowa throughout this night except for complicated patterns at 0201 UT. On the other hand, variations of neutral winds were rather independent of variations of plasma drifts.

[22] Time series of plasma drifts, neutral winds, and neutral temperatures are displayed in Figure 8. Since clear backscatter echoes were obtained in a limited area on 24–25 April, these time series are shown at two locations indicated as A and B at the bottom in this figure. In contrast to the 13 May case, there is no relationship between the variations of neutral winds and plasma drifts at both A and B. Moreover, by comparing the data at A with those at B, it is found that neutral wind velocities and temperatures and plasma drifts at A were more variable than those at B. This fact suggests that auroral activities at high magnetic latitude were more intense than those at low magnetic latitude since the magnetic latitude of location A is about 2° higher than that of B.

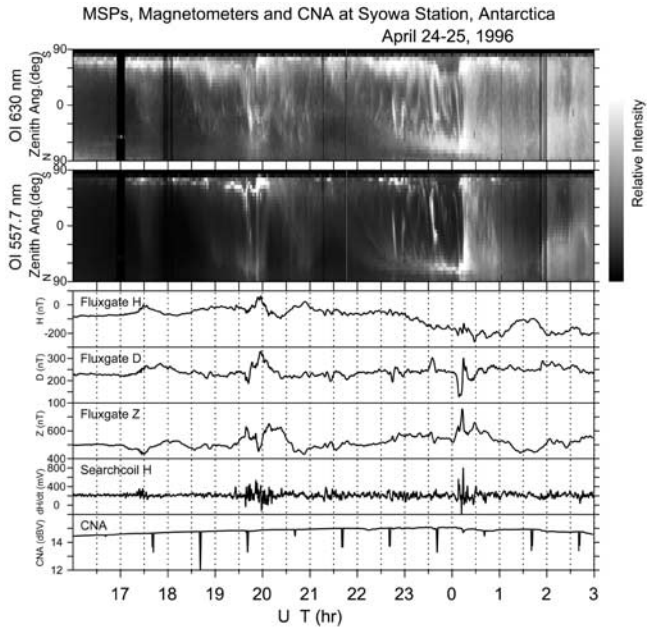

Figure 6. Summary plots of auroral and geomagnetic activities obtained on 24–25 April 1996 at Syowa. The format is the same as Figure 2.

4. Discussion

4.1. Backscatter Echoes Obtained by the Syowa-South HF Radar

[23] In the present study, plasma drifts in the *F* region were obtained from backscatter echoes of the Syowa-South HF radar in the range between 500 and 1000 km from Syowa Station. However, in previous studies, backscatter echoes from more distant ranges have been used in the estimation of *F* region plasma drifts [e.g., *Baker et al.*, 1995; *Watanabe et al.*, 1998]. First, we will confirm that the HF echoes used here are those scattered in the *F* region. *Hall et al.* [1997] demonstrated that near range (less than 400 km) echoes obtained by the SuperDARN radars are due to scattering of meteor trails [*Hall et al.*, 1997]. On the other hand, echoes used here were obtained in the range greater than 500 km. Moreover, Doppler shift velocities were 200–800 m/s as seen in Figures 5 and 8, compared with Doppler velocities less than 50 m/s given by *Hall et al.* [1997]. Consequently, we can conclude that the echoes used here are not due to scattering by meteor trails. Similarly, a possibility of auroral *E* region echoes are denied since these echoes are observed at ranges less than 400 km [*Hall et al.*, 1997; *Ogawa et al.*, 1990]. It would be, therefore, reasonable to conclude that the Doppler shift velocities of backscatter echoes used in this study represent the plasma drift speeds in the *F* region.

4.2. Ion-Neutral Coupling During Quiet and Moderate Active Periods

[24] We showed simultaneous neutral wind and plasma drift data obtained in two cases: one observed during a quiet

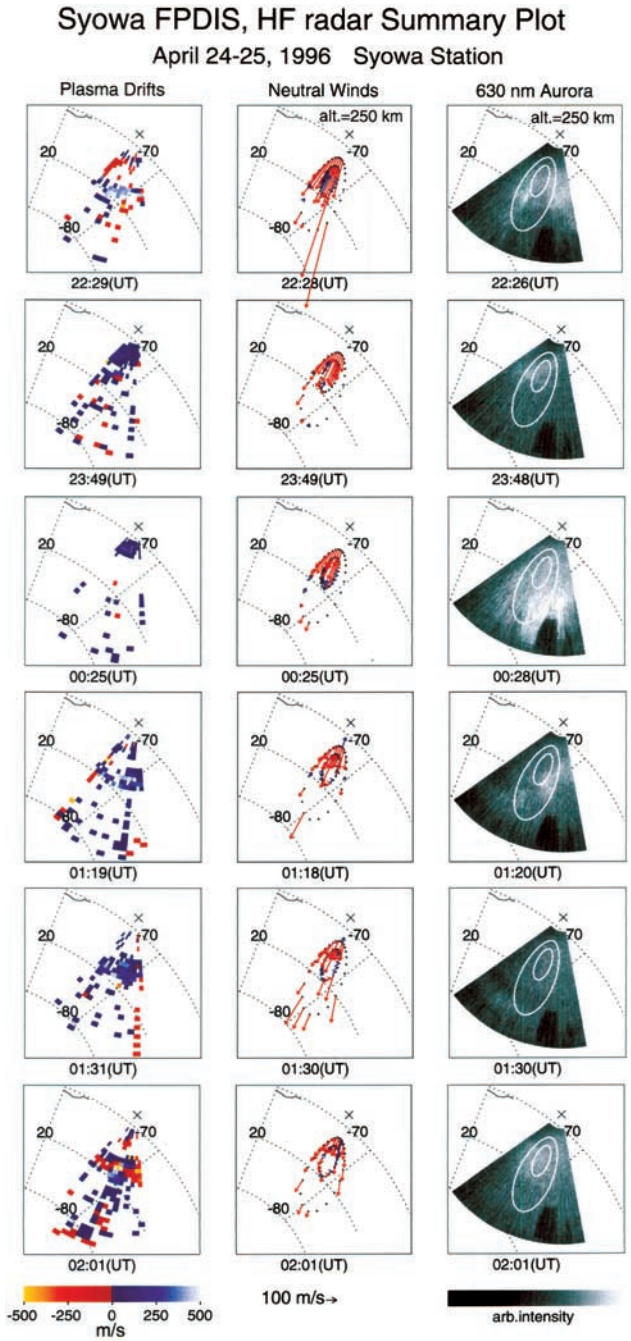

Figure 7. Summary plots of the simultaneous measurements between plasma drifts, neutral winds and auroral emission distributions at 630 nm obtained on 24–25 April 1996. The format is the same as Figure 3. Note that neutral winds at some sectors in the outer fringe were not estimated due to the low accuracy of the Gaussian fitting. In auroral images, a black circle was clearly identified around 77°S in latitude and 65°E in longitude, in particular at 0028 UT. This is due to a shadow of building in Syowa Station.

period including the growth phase of a substorm on 13 May 1996 and the other observed during a moderately active period on 24–25 April 1996. In the case of 13 May, the variations of neutral winds were closely related to those of plasma drifts. In contrast, there was no similarity between the variations of neutral winds and plasma drifts in the 24–25 April case.

[25] First, we will discuss the 13 May case in detail based on the time variations of neutral wind velocities and plasma drift velocities obtained at location C shown in Figure 5. Considering that the speeds of plasma drifts were about 7–10 times higher than those of neutral winds, and that the variations of plasma drifts preceded those of neutral winds with a time lag of 30 min, it is strongly suggested that neutral winds were driven by the ion drag force. The ratio of plasma drift speeds to neutral wind speeds (7–10) is greater

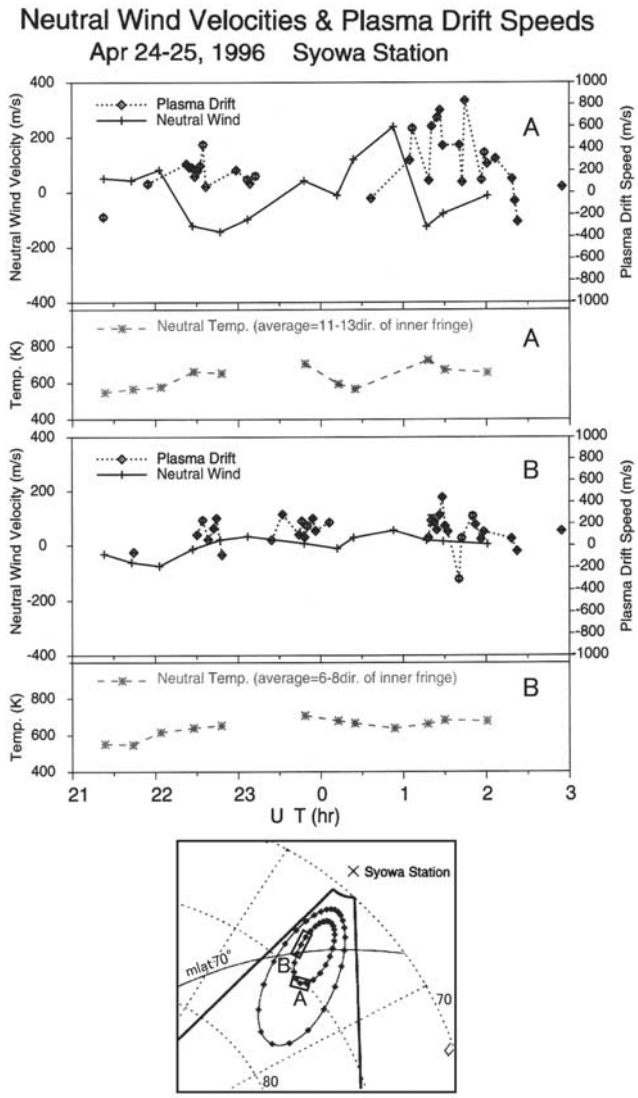

Figure 8. Time variations of simultaneous neutral wind velocities and plasma drift velocities in the line-of-sight direction at selected 2 locations obtained from 21 UT on 24 April to 3 UT on 25 April. The selected 2 locations indicated as A, B are shown in the bottom map. In neutral wind data, an average value was subtracted for wind data at each variation. The second and fourth panels show the variations of neutral temperatures obtained at locations A and B, respectively.

than the ratio of 3–5 obtained by DE-2 [*Killeen and Roble*, 1988]. This difference might be related to solar activity conditions since the data used in *Killeen and Roble* [1988] were obtained during the solar maximum period. Another important point to be considered is an apparent westward motion of the plasma drift pattern due to the Earth's rotation. Even if the plasma drift pattern such as convection reversal is stable with time, an apparent westward motion of the LOS velocity reversal region with an angular velocity due to the Earth's rotation would be observed by ground-based instruments. In this case, however, there is no time lag between the variations of neutral wind velocities and plasma drift velocities if the convection reversal is stable for the neutral-ion momentum transfer collision time (a few hours in the *F* region). The 13 May case is inconsistent with this case since a 30-min time lag was observed. Moreover, the speed of the westward motion of the plasma drift pattern (~60 m/s) obtained in the 13 May case is considerably less than the Earth's rotation speed at the latitude of Syowa (~240 m/s). Thus, it is concluded that the variations seen in the HF radar data were mainly due to the temporal variations of plasma drifts.

[26] To investigate the response of neutral wind to ion drag, we solved the momentum equation of horizontal neutral wind, and simulated several cases. The procedure used here is similar to that in the paper of *Thayer et al.* [1995a]. Our approach is based on the ground-based data obtained by the FPDIS and the HF radar concerning on the local dynamics in the thermosphere and ionosphere. In particular, the FPDIS observed the neutral winds at the altitude of auroral emission layer. Although it is well known that the altitude of aurora changes depending on the energy distribution of precipitating particles, the solar cycle dependence of aurora emission altitude may be unclear. Therefore, we have examined the dynamical coupling between neutrals and ions at the fixed altitude of 250 km. Since *Thayer et al.* [1995a] also used the ground-based FPI and digit-sonde data, we would consider that it is meaningful to compare our results of observations and calculations with those of *Thayer et al.* [1995a].

[27] The momentum equation of horizontal neutral wind in the upper atmosphere can be expressed by

$$\frac{\partial \vec{U}_n}{\partial t} = -\nu_{ni}(\vec{U}_n - \vec{V}_i) - \frac{\nabla P_n}{n_n m_n} - 2\Omega \sin\varphi\, \hat{k} \times \vec{U}_n - \vec{U}_n \cdot \nabla \vec{U}_n + \frac{\mu}{n_n m_n} \frac{\partial^2 \vec{U}_n}{\partial z^2} \quad (1)$$

where $\vec{U}_n$, $\vec{V}_i$ are the horizontal velocities of neutrals and ions, respectively, ν_{ni} the neutral-ion momentum transfer collision frequency, P_n the neutral pressure, n_n the number density of neutrals, m_n the mass of neutrals, μ the coefficient of viscosity, Ω the angular velocity of the Earth rotation, φ the latitude, and $\hat{k}$ the unit vector in the vertical direction. In this equation, the terms in the right hand side represent the ion drag force, the pressure gradient force, the Coriolis force, the momentum advection, and the viscosity in respective order.

[28] Here, only the ion drag and pressure gradient terms are taken into account in the calculation since we focus on the response of neutral winds to the ion drag force. This simplification would be valid for a short time interval under quiet conditions as in the 13 May case concerning on local ion-neutral coupling processes. Then, the horizontal neutral wind velocities in the line-of-sight direction are calculated since FPDIS and HF radar give information on neutral winds and plasma drifts, respectively, in the line-of-sight direction. Instead of the LOS plasma drift velocity, the horizontal plasma drift velocity should be used for estimating the horizontal neutral wind velocity. As described in section 2.2, the HF wave is generally scattered in the *F* region where the wave vector is almost perpendicular to the geomagnetic field. Considering that the waves emitted from the Syowa-South HF radar are almost directed magnetic poleward, the horizontal component of ion drift velocity is obtained by

$$V_i \approx V_{LOS} \cos(I)$$

where V_i and V_{LOS} are horizontal ion drift velocity and that of observed Doppler velocity in the LOS direction of HF radar, respectively, and I is the inclination of geomagnetic field at Syowa (=26).

[29] The densities and temperatures of neutrals used in this calculation are derived from the MSISE-90 model [*Hedin*, 1991], while the temperatures and densities of ions and electron are derived from the IRI-95 model [e.g., *Bilitza et al.*, 1993]. The altitude for those parameters is be 250 km, and therefore the calculation is made at the fixed altitude, not made at constant pressure levels. From the IRI-95 model, it is found that ion species in the *F* region consist of mainly oxygen and nitric oxide ions during this period. Thus, the neutral-ion collision frequency is estimated from the O-O^+ and the O-NO^+ collision frequencies by using the expression for the ion-neutral collision frequencies of O^+-O and NO^+-O given by *Shunk and Nagy* [1980] as follows

$$\nu_{in}(\mathrm{O^+ - O}) = 3.67 \times 10^{-11} n(\mathrm{O}) T_r^{1/2} (1 - 0.064 \log_{10} T_r)^2 \quad (2)$$

$$\nu_{in}(\mathrm{NO^+ - O}) = 2.44 n(\mathrm{O}) \quad (3)$$

where $T_r = (T_i + T_n)/2$; ν_{in}(O^+-O) and ν_{in}(NO^+-O) are O^+-O and NO^+-O collision frequencies, respectively; n(O) is the number density of atomic oxygen; T_i and T_n are temperatures of ions and neutrals, respectively. Then, the relation

$$\nu_{ni}(\mathrm{O - O^+}) = \frac{n(\mathrm{O^+}) m(\mathrm{O^+})}{n(\mathrm{O}) m(\mathrm{O})} \nu_{in}(\mathrm{O^+ - O}) \quad (4)$$

is used for the O-O^+ collision frequency, and similar relation is valid for the O-NO^+ collision frequency. Finally we obtain the neutral-ion collision frequency by

$$\nu_{ni} = \nu_{ni}(\mathrm{O - O^+}) + \nu_{ni}(\mathrm{O - NO^+}). \quad (5)$$

Further, the pressure gradient force along the line-of-sight direction is estimated from number densities and temperatures of O and N_2 using the MSISE-90 model. Thus, this term represents a large-scale pressure gradient force such as the day-to night pressure gradient.

[30] Figure 9a shows calculated neutral wind velocities by solid curves and the horizontal velocities of observed

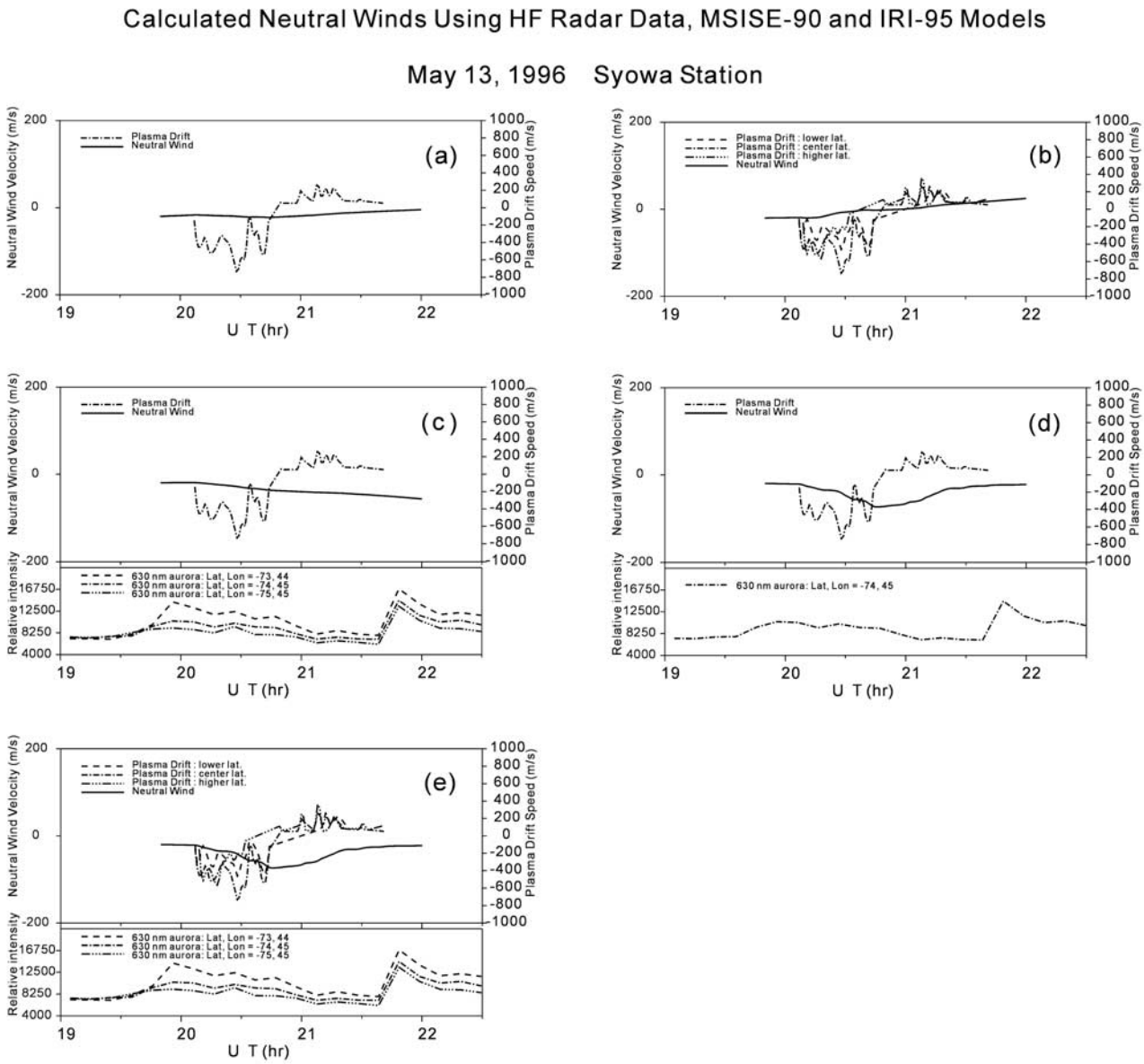

Figure 9. Calculated horizontal neutral wind velocities from plasma drift and auroral intensity data obtained on 13 May 1996 with four conditions shown in the following: (a) No heating effect is included. The ion drag and pressure gradient force were estimated from the MSISE-90 and IRI-95 models. (b) The Joule heating is only included. Time variations of the observed plasma drifts at the three locations are shown in the bottom panel. (c) The particle heating is only included. The time variations of the observed 630 nm aurora intensities at the three locations are plotted in the bottom panel. (d) The increase of ion density is only included. (e) All the effects, that is, particle and Joule heating and increases of ion densities, are included.

plasma drift indicated by dashed-dotted curves. Here, the start time of calculation is 1950 UT with an initial neutral wind speed of −20 m/s, referring to the observed neutral winds in Figure 5c. Compared with the observed neutral winds, calculated neutral winds are found to be very small with a peak of negative excursion of −23.7 m/s at 2044 UT. Thus, the ion drag force has little effect for driving neutral winds due to an extremely small value of the neutral-ion frequency. From MSISE-90 model, it is found that temperatures and number densities of ions and neutrals at an altitude of 250 km are lower at solar minimum than at solar maximum, although the solar cycle dependence of neutral density is rather smaller than that of ion density. As a result of those small temperatures and number densities, the neutral-ion frequency shows an extremely small value. Here, the maximum of the neutral-ion collision frequency is estimated to be 1.34×10^{-5} Hz which is about 7–8 times smaller than the collision frequency at solar maximum shown by *Thayer et al.* [1995a]. Moreover, from MSISE-90 model, the pressure gradient force is estimated to be -0.003 m/s^2 which is also about 17 times smaller than the pressure gradient force obtained by *Thayer et al.* [1995a]

using the VSH model. Thus, in Figure 9a we cannot identify the effect of the pressure gradient force. It is interesting to find that the response of neutrals to ions is quite different between two conditions of the solar minimum and maximum.

[31] From the fact that calculated neutral winds show much smaller variations than observed neutral winds, it is suggested that parameters used for the global thermosphere-ionosphere models are not appropriate in the present local coupling model of neutrals and ions, and that increases in temperatures of both neutrals and ions must occur in the 13 May case even though auroral activity is low. Temperature increases might occur associated with diffuse aurora existing poleward of Syowa as seen in Figures 2 and 3.

[32] Next we show the Joule and particle heating effects to the ion-neutral coupling in this case. As represented in equations (2)–(4), the neutral-ion collision frequency depends on T_n, T_i, and, $n_i(= n(O^+) + n(NO^+))$, while the pressure gradient depends on T_n and n_n. Although the neutral temperatures were observed by FPDIS, the absolute values of observed neutral temperatures were not validated, as described in the data analysis. Therefore, we assume that temperature increases due to Joule heating are represented by

$$\Delta T_n/\Delta t = \Delta T_i/\Delta t = \alpha E(t)^2 \tag{6}$$

where $E(t)$ is the magnitude of electric field at a certain time derived from the HF radar data, and α is a constant, since the Joule heating rate is given by $Q = \sigma_p|\vec{E}|^2$ where σ_p is the Pedersen conductivity. Here, the magnitude of electric field E from HF radar data is used instead of that of electric field vector since there is no electric field data aligned with the radar beam. We take notice that the magnitude of electric field E derived from the HF radar data is usually smaller than that of electric field vector since the observed LOS velocity gives only an electric field component perpendicular to the radar beam. Although an error might be caused due to this simple assumption used here, we could examine the effect Joule heating on this event. On the other hand, the energy spectrum of precipitating particles should be needed to estimate the particle heating effect. However, in this event we have no precipitating particle data obtained simultaneously by a satellite or another instrument. Therefore, it is assumed that that the intensity of auroral emission is roughly proportional to the energy flux of precipitating particles. Then, we simply infer that increase in temperature is roughly proportional to the auroral intensity to estimate the particle heating as follows

$$\Delta T_n/\Delta t = \Delta T_i/\Delta t = \beta I_{630}(t) \tag{7}$$

where $I_{630}(t)$ is the OI 630 nm auroral intensity observed by the monochromatic imager at a certain time, while β is a constant. We should take notice that the proportionality would be lost if low energy particle heating might often contribute to the temperature change. The increased temperatures are calculated from the observed electric fields and auroral intensities at three locations: C in Figure 5 and $\sim 1^\circ$ higher and $\sim 1^\circ$ lower latitude points in the line-of-sight direction. Then the pressure gradient force is estimated. Further, increases in number densities for ions are assumed by

$$\Delta n(O^+)/\Delta t = \Delta n(NO^+)/\Delta t = \gamma I_{630}(t) \tag{8}$$

where γ is a constant. Although our approach with these simple assumptions is not based on rigorous scientific models, we can test the effects of auroral heating and estimate the temperature increase that is required for producing the observed neutral winds.

[33] Figures 9b–9e show the calculated results of neutral winds driven by the horizontal component of observed ion drifts including additional heating effects such as Joule and particle heating, and increases in ion number densities. Figure 9b represents the time variations of neutral winds in the case that the Joule heating effect shown in equation (6) is only included. Figure 9c simulates neutral winds in the case that the particle heating effect shown in equation (7) is only included. The time variations of the observed 630 nm aurora intensities at the three locations used in the calculations are plotted in the bottom. Further, Figure 9d simulates neutral winds in the case that the increase of ion density shown in equation (8) is only included. The time variations of the observed 630 nm aurora intensities used in the calculations are plotted in the bottom. Finally, Figure 9e shows the time variation of neutral winds in the case that all the effects, that is, particle and Joule heating and increase of ion density, are included. It is found in Figure 9b that the acceleration due to Joule heating is slightly positive throughout the period. In contrast, as seen in Figure 9c that particle heating contributes to acceleration of the negative excursion of neutral winds. We interpret that the neutral wind acceleration seen in Figures 9b and 9c are mainly caused by enhanced pressure gradient force due to the effects of Joule and particle heating, respectively. On the other hand, the negative excursion of neutral winds reaching about -85 m/s at $\sim$2045 UT followed by a positive excursion is seen in Figure 9d, suggesting that the ion drag force is enhanced due to the increase of ion density. Consequently, as shown in Figure 9e, the negative and acceleration of neutral winds is well reproduced. However, compared with the observed neutral wind variations shown in Figure 5c, it is difficult to reproduce the quick recovery of neutral winds from these calculations. This discrepancy is discussed later.

[34] The parameters with heating effects used in this calculation are summarized in Table 1. As seen in Table 1, the maximum values of T_n and T_i are about 150 K higher than those in the MSISE-90 and IRI 95-models. Those temperature increases of ions and neutrals are often seen associated with auroral activities [*Oyama et al.*, 2001]. Also the neutral-collision frequency is about 20 times greater than the value without heating. From these calculations, it is still unclear which effect among Joule and particle heating and ion density increase was dominant to generate actual neutral wind variations since the factors α, β and γ are not based on rigorous scientific models. However, we consider that the ion drag is important on the two points in the following: (1) The ion drag force can generate the similar variation between neutral winds and plasma drifts shown in this study, although pressure gradient and remote global

Table 1. Values of the Parameters Without Heating (Left-Hand Column) and With Effects of Particle and Joule Heating (Right-Hand Column)[a]

	No Heating	Maximum Value With Heating
Neutral temperature	629.1 K	783 K
Ion temperature	663.9 K	817 K
Neutral-ion collision frequency	1.34×10^{-5} Hz	2.7×10^{-4} Hz
Pressure gradient force	-0.0030 m/s^2	-0.0195 m/s^2
Ion drag force	-0.0107 m/s^2	-0.0601 m/s^2

[a] The parameters used are neutral and ion temperatures, the neutral-ion collision frequencies, the pressure gradient force, and the ion drag force. On the parameters in the case including heating effects, and ion drag force in the case without heating, the maximum value is indicated.

force may accidentally produce the similar variation. (2) From the calculations, it is difficult to reproduce the quick recovery of neutral winds observed after ~2045 UT. If the ion drag acceleration is greater than that used in the calculations, this quick recovery of neutral winds ca be reproduced. To drive such positive acceleration of neutral winds, the ion drag force may play an important role since the direction of ion drag force changed from negative to positive after ~2045 UT.

[35] In this event analysis, the equations are solved locally rather than globally since we have concerned on local neutral-ion coupling processes. Thus, it is suggested that the recovery of neutral winds observed after 2045 UT is driven by ion drag force. However, if large-scale remote forces, such as the advection, are comparable or greater than local forces, the remote forces would have a substantial influence on the local dynamics. Specifically, in the recovery phase of neutral winds observed after 2045 UT, the discrepancy between observed and simulated winds might be caused by the large-scale remote forces. It is difficult to examine the influence of global remote forces on local processes in this study, and further study would be needed to clarify the relationship between local and global processes by using ground-based observation data and global-scale data obtained by a satellite data and TGCM-class models.

[36] Here, the validity of time lag of ~30 min between the variations of neutral winds and plasma drifts is discussed. In the momentum equation (1), we consider that the ion drag force is the only term to accelerate the neutral winds and also that the ion velocity is constant. Then, the solution of the equation for the LOS component is expressed by [*Thayer et al.*, 1995a]

$$U_n = (U_{n0} - V_i)e^{-\nu_{ni}t} + V_i \tag{9}$$

where U_n and V_i are the horizontal velocities of neutrals and ions, respectively, the subscript 0 indicates a constant. In this case, it is probable that the time lag between the velocities of neutral wind and ion drift may be determined by the time when the neutral wind velocity is changed by a factor of $1/e$. Hence, the time lag may be equal to $1/\nu_{ni}$. Since the neutral-ion collision frequency used in the calculation including the heating effects is 2.7×10^{-4} Hz, the estimated time lag is about 60 min, which is two times greater than that obtained from observed data. Considering the fact that the recovery of the observed neutral wind was more quick than that of calculated neutral wind, this discrepancy between the two time lag values is consistent, and therefore support the existence of further pressure gradient and ion drag force and/or global remote forces, as discussed above.

[37] Next, we discuss the features of neutral winds and plasma drifts observed on 24–25 April 1996 when there was no similarity between neutral winds and plasma drifts. As described in the results, the auroral conditions in the 24–25 April case were more active than in the 13 May case. Although it is difficult to specify reasons for different time variations between neutral winds and plasma drifts, here we propose some possible origins as follows. First, if the pressure gradient force of neutrals is much greater than the ion drag force, neutral winds show variations independent of plasma drifts. In particular, the local pressure gradient force generated by fluctuated auroral heating would produce complicated neutral wind structures. Second, there is a possibility that different behaviors of neutral winds and plasma drifts are caused by vertical neutral winds. In this study, we considered the LOS velocity obtained by FPDIS as the horizontal wind velocity assuming that vertical winds were negligible. However, as pointed out by *Conde and Smith* [1998] significant vertical winds often occur in the late evening to midnight sector. Further, *Ishii et al.* [2001] suggested that upward and downward winds with a maximum velocity of ~50 m/s occurred in association with active aurora. From simple geometric estimation, it is obvious that the LOS component of vertical wind is equal to, $U_v \cos\theta$ where U_v is the vertical wind velocity and θ is the zenith angle of observation point. Then, the error in $U_v/\tan\theta$ arises in the horizontal wind velocity estimated from observed data assuming that the vertical wind velocity is zero. For example, if the vertical wind velocity is 50 m/s and $\theta = 60°$, the error in the horizontal wind velocity is 29 m/s. Especially, a discrepancy between neutral winds and plasma drifts observed around ~0100 UT on 25 April might be caused by vertical winds associated with an auroral breakup occurring at 0015 UT. Third, there is a possibility that the error in neutral wind velocity is induced by the shift of fringe peak position due to a large gradient of auroral intensity in the FOV of FPDIS during the active period on 24–25 April. As described above, further observations would be needed to identify the origins of the complicated relationships between neutral winds and plasma drifts during the active period. For example, we need (1) accurate estimations of the effect of auroral heating, such as the estimations from IS radar data, (2) simultaneous observations of horizontal and vertical winds, (3) accurate corrections of the large gradient of auroral intensity in Fabry-Perot imager data.

5. Summary

[38] In order to investigate the local dynamical coupling between neutrals and ions in the auroral *F* region during the solar minimum period, we observed thermospheric winds and plasma drifts using the FPDIS and the Syowa-South HF radar, respectively, at Syowa Station (66.4° in magnetic latitude), Antarctica. We made case studies using simultaneous neutral wind and plasma drift data observed on 13

May 1996 during a quiet period including the growth phase of a substorm, and 24–25 April 1996 during a moderately active period. The obtained results are summarized as follows:

1. From ~2000 to 2200 UT on 13 May, both velocities of neutral winds and plasma drifts showed similar time variations. The neutral wind velocities varied in the range from ~−80 to +60 m/s, while plasma drift velocities varied in the range from ~−850 to 400 m/s at the same locations. Thus, plasma drift velocities were about 7–10 times greater than neutral wind velocities. It is also found that there is a good correlation between the neutral wind acceleration and the plasma drift velocity. Further, the variations of plasma drift velocities preceded those of neutral wind velocities with a time lag of 30 min. Therefore, it is strongly suggested that the variations of neutral winds were driven by the ion drag force.

2. To investigate the response of neutral winds to the ion drag, we solved the momentum equation for horizontal wind in the 13 May case and simulated the relationship between neutral winds and plasma drifts with some assumptions. It was found that that the velocities of neutral wind driven by the ion drag force and the pressure gradient force estimated from the MSISE-90 and IRI-95 models are much weaker than observed neutral wind velocities. Thus, it is suggested that the ion drag and the pressure gradient force are underestimated. Here, the estimated neutral-ion collision frequency is $1.34 \times 10^{-}5$ Hz which is about 7–8 times smaller than the collision frequency at solar maximum presented by *Thayer et al.* [1995a], while the estimated pressure gradient force is -0.003 m/s^2 which is also about 17 times smaller than that given by *Thayer et al.* [1995a].

3. Considering the auroral heating effects with assumptions that the temperature increase due to Joule heating is proportional to the square of observed electric fields, and that the temperature increase due to particle heating and an ion density increase are proportional to the 630 nm auroral intensity, the negative acceleration of neutral winds is well reproduced by a calculation with a maximum temperature increase of ~150 K. It is, therefore, suggested that significant neutral winds were driven by the ion drag and the pressure gradient force due to Joule/particle heating. However, in this calculation the ion drag force might be underestimated since positive acceleration of neutral wind velocity observed after ~2045 UT is not well reproduced. Regarding other candidates for the positive acceleration of neutral winds, large-scale remote forces, such as the advection, might contribute to the recovery of neutral winds. However, it is difficult to examine the effect of global remote forces in this study since we have concerned on the local-scale neutral-ion coupling using ground-based observation data. The time lag between variations of neutral winds and ion drifts is about 60 min estimated from the neutral-ion collision frequency used in the calculation is 2.7×10^{-4} Hz including the heating effects, and therefore the estimated time lag is about two times greater than that seen in observed data. This discrepancy also supports the existence of further pressure gradient and ion drag force and/or global remote forces.

4. In contrast, from a case study on 24–25 April during the moderate active period, there was no similarity between the behaviors of neutral winds and plasma drifts. In particular, during the active period after an auroral breakup at 0015 UT on 25 April, we see there was a significant discrepancy between neutral winds and plasma drifts. Although it is difficult to specify the sources for the discrepancy, possible origins were proposed. If the pressure gradient force of neutrals is much greater than the ion drag force, neutral winds show variations independent of plasma drifts. Moreover, discrepancy may be caused by vertical winds since we considered the line-of-sight velocity obtained by FPDIS as the horizontal wind velocity assuming that vertical winds were negligible.

[39] **Acknowledgments.** We thank Masakazu Watanabe for his assistance in handling the Syowa HF radar data. We thank all members of the 37th wintering party of Japanese Antarctic Research Expedition for their support at Syowa Station. MSP and Geomagnetic data were provided by the World Data Center-C2 for aurora in National Institute of Polar Research. The Ministry of Education, Culture, Sports, Science, and Technology (MONBUKAGAKUSHO) supported the Syowa HF radar system. The research for HF radar was supported by a Grant-in Aid for Scientific Research (A) from Japan Society for the Promotion of Science (JSPS). IMF conditions obtained by the WIND spacecraft were downloaded from the "cdaweb" service site, http://cdaweb.gsfc.nasa.gov/cdaweb/istp_public. The MSISE-90 and IRI-95 models were obtained from the Web pages of NASA's National Space Science Data Center.

References

Baker, K. B., J. R. Dudeney, R. A. Greenwald, M. Pinnock, P. T. Newell, A. S. Rodger, N. Mattin, and C.-I. Meng, HF radar signatures of the cusp and low-latitude boundary layer, *J. Geophys. Res.*, *100*, 7671–7695, 1995.

Batten, S. D., and D. Rees, Thermospheric winds in the auroral oval: Observations of small scale structures and rapid fluctuations by a Doppler imaging system, *Planet. Space Sci.*, *38*, 675–694, 1990.

Bilitza, D., K. Rawer, L. Bossy, and T. Gulyaeva, International reference ionosphere-past, present, future, *Adv. Space Res.*, *13*, 3–23, 1993.

Brinkman, D. G., R. L. Walterscheid, L. R. Lyons, D. C. Kayser, A. B. Christensen, J. R. Sharber, R. A. Frahm, and M. F. Larsen, E region neutral winds in the postmidnight diffuse aurora during the Atmospheric Response in Aurora 1 rocket campaign, *J. Geophys. Res.*, *100*, 17,309–17,320, 1995.

Conde, M., and R. W. Smith, Mapping thermospheric winds in the auroral zone, *Geophys. Res. Lett.*, *22*, 3019–3022, 1995.

Conde, M., and R. W. Smith, Spatial structure in the thermospheric horizontal wind above Poker Flat, Alaska, during solar minimum, *J. Geophys. Res.*, *103*, 9449–9471, 1998.

Conde, M., et al., Assimilated observations of thermospheric winds, the aurora, and ionospheric currents over Alaska, *J. Geophys. Res.*, *106*, 10,493–10,508, 2001.

Deng, W., T. L. Killeen, A. G. Burns, R. G. Roble, J. A. Slavin, and L. E. Wharton, The effects of neutral inertia on ionospheric currents in the high-latitude thermosphere following a geomagnetic storm, *J. Geophys. Res.*, *98*, 7775–7790, 1993.

Dyson, P. L., T. P. Davies, M. L. Parkinson, A. J. Reeves, P. G. Richards, and C. E. Fairchild, Thermospheric neutral winds at southern mid-latitudes: A comparison of optical and ionosonde h_mF_2 methods, *J. Geophys. Res.*, *102*, 27,189–27,196, 1997.

Freeman, M. P., J. M. Ruohomiemi, and R. A. Greenwald, The determination of time-stationary two-dimensional convection patterns with single-station radars, *J. Geophys. Res.*, *96*, 15,735–15,749, 1991.

Fujii, R., S. Nozawa, N. Matuura, and A. Brekke, Study on neutral winds contribution to the electrodynamics in the polar ionosphere using EISCAT CP-1 data, *J. Geophys. Res.*, *103*, 14,731–14,739, 1998a.

Fujii, R., S. Nozawa, S. C. Buchert, N. Matuura, and A. Brekke, The motion of ions in the auroral ionosphere, *J. Geophys. Res.*, *103*, 20,685–20,695, 1998b.

Fujii, R., S. Nozawa, S. C. Buchert, and A. Brekke, Statistical characteristics of electromagnetic energy transfer between the magnetosphere, the ionosphere, and the thermosphere, *J. Geophys. Res.*, *104*, 2357–2365, 1999.

Fuller-Rowell, T. J., M. V. Codrescu, R. J. Moffett, and S. Quegan, Response of the thermosphere and ionosphere to geomagnetic storms, *J. Geophys. Res.*, *99*, 3893–3914, 1994.

Greenwald, R. A., et al., DARN/SuperDARN: A global view of the dynamics of high-latitude convection, *Space Sci. Rev.*, *71*, 761–796, 1995.

Hall, G. E., J. W. MacDougall, D. R. Moorcroft, J.-P. St.-Maurice, A. H. Manson, and C. E. Meek, Super Dual Auroral Radar Network observations of meteor echoes, *J. Geophys. Res.*, *102*, 14,603–14,614, 1997.

Hays, P. B., T. L. Killeen, N. W. Spencer, L. W. Wharton, R. G. Roble, B. A. Emery, T. J. Fuller-Rowell, D. Rees, L. A. Frank, and J. D. Craven, Observations of the dynamics of the polar thermosphere, *J. Geophys. Res.*, *89*, 5597–5612, 1984.

Hedin, A. E., Extension of the MSIS thermospheric model into the middle and lower atmosphere, *J. Geophys. Res.*, *96*, 1159–1172, 1991.

Hernandez, G., R. W. Smith, R. G. Roble, J. Gress, and K. C. Clark, Thermospheric dynamics at the south pole, *Geophys. Res. Lett.*, *17*, 1255–1259, 1990.

Ishii, M., S. Oyama, S. Nozawa, R. Fujii, E. Sagawa, S. Watari, and H. Shinagawa, Dynamics of neutral wind in the polar region observed with two Fabry-Perot interferometers, *Earth Planet. Sci.*, *51*, 833–844, 1999.

Ishii, M., M. Conde, R. W. Smith, M. Krynicki, E. Sagawa, and S. Watari, Vertical wind observations with two Fabry-Perot interferometers at Poker Flat, Alaska, *J. Geophys. Res.*, *106*, 10,537–10,552, 2001.

Killeen, T. L., and P. B. Hays, Doppler line profile analysis for a multichannel Fabry-Perot interferometer, *Appl. Opt.*, *23*, 612–620, 1984.

Killeen, T. L., and R. G. Roble, An analysis of the high-latitude thermospheric wind pattern calculated by a thermospheric general circulation model, 1, Momentum forcing, *J. Geophys. Res.*, *89*, 7509–7522, 1984.

Killeen, T. L., and R. G. Roble, Thermospheric dynamics: Contributions from the first 5 years of the Dynamics Explorer program, *Rev. Geophys.*, *26*, 329–367, 1988.

Killeen, T. L., P. B. Hays, G. R. Carignan, R. A. Heelis, W. B. Hanson, N. W. Spencer, and L. H. Brace, Ion-neutral coupling in the high-latitude F-region: Evaluation of ion heating terms from Dynamics Explorer 2, *J. Geophys. Res.*, *89*, 7495–7508, 1984.

Killeen, T. L., R. A. Heelis, P. B. Hays, N. W. Spencer, and W. B. Hanson, Neutral motions in the polar thermosphere for northward interplanetary magnetic field, *Geophys. Res. Lett.*, *12*, 159–162, 1985.

Kubota, M., A study on middle-scale variations of thermospheric neutral winds associated with auroral activity over Syowa Station, Antarctica, Doctoral thesis, Tohoku Univ., Sendai, Japan, 1996.

Lu, G., A. D. Richmond, B. A. Emery, and R. G. Roble, Magnetosphere-ionosphere coupling: Effect of neutral wind on energy transfer and field-aligned current, *J. Geophys. Res.*, *100*, 19,643–19,659, 1995.

Lyons, L. R., and R. L. Walterscheid, Generation of auroral omega bands by shear instability of neutral winds, *J. Geophys. Res.*, *90*, 12,321–12,329, 1985.

Nakajima, H., S. Okano, H. Fukunishi, and T. Ono, Observations of thermospheric wind velocities and temperatures by the use of a Fabry-Perot Doppler imaging system at Syowa Station, Antarctica, *Appl. Opt.*, *34*, 8382–8395, 1995.

Odom, C. D., M. F. Larsen, A. B. Christensen, P. C. Anderson, J. H. Hecht, D. G. Brinkman, R. L. Walterscheid, L. R. Lyons, R. Pfaff, and B. A. Emery, ARIA II neutral flywheel-driven field-aligned currents in the postmidnight sector of the auroral oval: A case study, *J. Geophys. Res.*, *102*, 9749–9759, 1997.

Ogawa, T., T. Hirasawa, M. Ejiri, N. Sato, H. Yamagichi, R. Fujii, and K. Igarashi, HF radar experiment at Syowa Station for the study of high-latitude ionosphere, 2, A capability (extended abstract), *Proc. NIPR Symp. Upper Atmos. Phys.*, *3*, 91–95, 1990.

Oyama, S. M. Ishii, Y. Murayama, H. Shinagawa, S. C. Buchert, R. Fujii, and W. Kofman, Generation of atmospheric gravity waves associated with auroral activity in the polar *F* region, *J. Geophys. Res.*, *106*, 18,543–18,554, 2001.

Peymirat, C., A. D. Richmond, B. A. Emery, and R. G. Roble, A magnetosphere-thermosphere-ionosphere electrodynamics general circulation model, *J. Geophys. Res.*, *103*, 17,467–17,477, 1998.

Rees, D., A. H. Greenway, R. Gordon, I. McWhirter, P. J. Charleton, and Steen, The Doppler imaging system: Initial observations of the auroral atmosphere, *Planet. Space Sci.*, *32*, 273–285, 1984.

Ruohomiemi, J. M., R. A. Greenwald, K. B. Baker, J.-P. Vallain, C. Hanuise, and J. Kelly, Mapping high-latitude plasma convection with coherent HF radars, *J. Geophys. Res.*, *94*, 13,463–13,477, 1989.

Sakanoi, T., and H. Fukunishi, Observations of vertical winds in the thermosphere with a Fabry-Perot Doppler imager at Syowa Station, Antarctica, *Adv. Space Res.*, *24*, 1439–1442, 1999.

Shunk, R. W., and A. F. Nagy, Ionospheres of the terrestrial planets, *Rev. Geophys. Space Phys.*, *18*, 813–852, 1980.

Smith, R. W., G. Hernandez, K. Price, G. Fraser, K. C. Clark, W. J. Schulz, S. Smith, and M. Clark, The June 1991 thermospheric storm observed in the southern hemisphere, *J. Geophys. Res.*, *99*, 17,609–17,615, 1994.

Solomon, S. C., P. B. Hays, and V. J. Abreu, The auroral 6300A emission: Observations and modeling, *J. Geophys. Res.*, *93*, 9867–9882, 1988.

Steen, D. Rees, P. N. Collis, and J. S. Murphree, What role does the F-region neutral wind play in auroral intensifications?, *Planet. Space Sci.*, *26*, 851–868, 1988.

Sun, Z.-P., R. P. Turco, R. L. Walterscheid, S. V. Venkateswaran, and P. W. Jones, Thermospheric response to morningside diffuse aurora: High-resolution three-dimensional simulations, *J. Geophys. Res.*, *100*, 23,779–23,793, 1995.

Thayer, J. P., G. Crowley, R. H. Niciejewski, T. L. Killeen, J. Buchau, and B. W. Reinisch, Ground-based observations of ion/neutral coupling at Thule and Qanaq, Greenland, *J. Geophys. Res.*, *100*, 12,189–12,199, 1995a.

Thayer, J. P., J. F. Vickrey, R. A. Heelis, and J. B. Gary, Interpretation and modeling of the high-latitude electromagnetic energy flux, *J. Geophys. Res.*, *100*, 19,715–19,728, 1995b.

Walterscheid, R. L., and L. R. Lyons, The neutral circulation in the vicinity of a stable auroral arc, *J. Geophys. Res.*, *97*, 19,489–19,499, 1992.

Watanabe, M., M. Pinnock, A. S. Rodger, N. Sato, H. Yamagishi, A. S. Yukimatu, R. A. Greenwald, J.-P. Villain, and M. R. Hariston, Localized activation of the distant tail neutral line just prior to substorm onsets, *J. Geophys. Res.*, *103*, 17,651–17,669, 1998.

H. Fukunishi, S. Okano, and T. Sakanoi, Department of Geophysics, Graduate School of Science, Tohoku University, Sendai 980-0845, Japan. (tsakanoi@pparc.geophys.tohoku.ac.jp)

N. Sato, H. Yamagishi, and A. S. Yukimatu, National Institute of Polar Research, Kaga, Itabashi, Tokyo, Japan.